

RECENT LHCb SPECTROSCOPY RESULTS*

ANTIMO PALANO

on behalf of the LHCb Collaboration

INFN and University of Bari, Italy

(Received December 5, 2014)

Studies of B and B_s decays having a J/ψ in the final state have been performed which allow new measurements on the scalar and axial mesons mixing angles. Two new natural parity and two unnatural parity resonances are observed in the inclusive study of $D^+\pi^-$, $D^0\pi^+$ and $D^{*+}\pi^-$ final states. In a Dalitz plot analysis of $B_s^0 \rightarrow \bar{D}^0 K^- \pi^+$, an excess at $m(\bar{D}^0 K^-) \approx 2.86 \text{ GeV}/c$ is found to be an admixture of spin-1 and spin-3 resonances. The analyses make use of data corresponding to 3 fb^{-1} of integrated luminosity collected with the LHCb detector using pp collisions.

DOI:10.5506/APhysPolBSupp.8.159

PACS numbers: 14.40.Be, 14.40.Lb, 14.40.Nd

1. Light meson spectroscopy in B and B_s^0 decays

The decays of B and B_s mesons to $J/\psi X$ are useful for obtaining new information on the structure of the light mesons. In particular, tests have been proposed to ascertain if the scalar $f_0(500)$ and $f_0(980)$ mesons are formed of $q\bar{q}$ or tetraquarks [1]. Comparison between B and B_s mesons decays allow the measurement of mixing angles even if the mixing particle is not known.

1.1. Measurement of the resonant components in $\bar{B}^0 \rightarrow J/\psi\pi^+\pi^-$ decays

In this analysis, we measure the resonant substructure of the $\bar{B}^0 \rightarrow J/\psi\pi^+\pi^-$ decay [2]. Optimization of the signal-to-background ratio in the reconstruction of B^0 meson, was performed through a BDT [3] algorithm which make use of samples of signal Monte Carlo events and real data for the

* Talk presented at the EEF70 Workshop on Unquenched Hadron Spectroscopy: Non-Perturbative Models and Methods of QCD *vs.* Experiment, Coimbra, Portugal, September 1–5, 2014.

background. The invariant mass of the selected $J/\psi\pi^+\pi^-$ combinations is shown in Fig. 1 (left). The mass fit gives $18\,841 \pm 204$ signal and $10\,207 \pm 178$ background candidates within ± 20 MeV of the \bar{B}^0 mass peak.

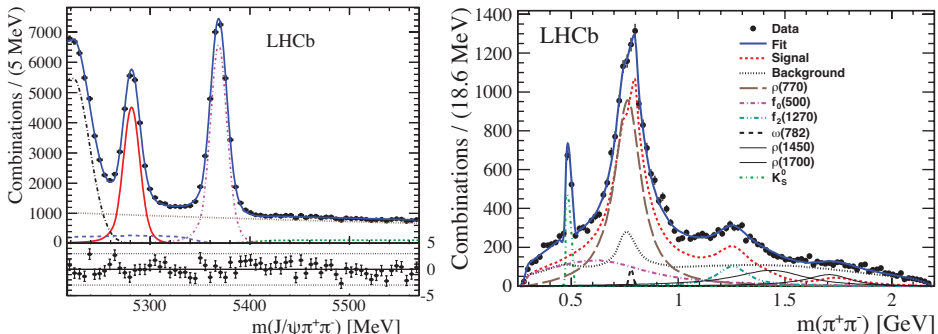


Fig. 1. $\bar{B}^0 \rightarrow J/\psi\pi^+\pi^-$. Left: Invariant mass of $J/\psi\pi^+\pi^-$ combinations together with the \bar{B}^0 data fit. Right: Fit projection of $m(\pi^+\pi^-)$ showing the different resonant contributions.

A Dalitz plot analysis which include information from the $J/\psi \rightarrow \mu^+\mu^-$ has been performed. The results from the fit are shown in Fig. 1 (right) and fit fractions are displayed in Table I. The decay is dominated by the $\rho(770)$ and $f_0(500)$ resonances, with little evidence for an $f_0(980)$ contribution.

TABLE 1

Fit fractions from the Dalitz plot analysis of $\bar{B}^0 \rightarrow J/\psi\pi^+\pi^-$.

Component	Fit fraction [%]
$\rho(770)$	$63.1 \pm 2.2^{+3.4}_{-2.2}$
$f_0(500)$	$22.2 \pm 1.2^{+2.6}_{-3.5}$
$f_2(1270)$	$7.5 \pm 0.6^{+0.4}_{-0.6}$
$\omega(782)$	$0.68^{+0.20+0.17}_{-0.14-0.13}$
$\rho(1450)$	$11.6 \pm 2.8 \pm 4.7$
$\rho(1700)$	$5.1 \pm 1.2 \pm 3.0$

The substructure of mesons belonging to the scalar nonet is controversial. Most mesons are thought to be formed from a combination of a q and a \bar{q} but some authors introduce the concept of $q\bar{q}q\bar{q}$ states. In either case, the $I = 0$ $f_0(500)$ and the $f_0(980)$ are thought to be mixtures of the underlying states whose mixing angle has been estimated previously. In the $q\bar{q}$ model, the mixing is parameterized by a normal 2×2 rotation matrix characterized

by the angle φ_m . The mixing angle is given by

$$\tan^2 \varphi_m \equiv r_\sigma^f = \frac{\mathcal{B}(\bar{B}^0 \rightarrow J/\psi f_0(980)) \Phi(500)}{\mathcal{B}(\bar{B}^0 \rightarrow J/\psi f_0(500)) \Phi(980)}, \quad (1)$$

where the Φ s are phase space factors [1] and we set $\frac{\Phi(500)}{\Phi(980)} = 1.25$. The fit gives the ratio of branching fractions

$$\frac{\mathcal{B}(\bar{B}^0 \rightarrow J/\psi f_0(980), f_0(980) \rightarrow \pi^+\pi^-)}{\mathcal{B}(\bar{B}^0 \rightarrow J/\psi f_0(500), f_0(500) \rightarrow \pi^+\pi^-)} = \left(0.6_{-0.4}^{+0.7+3.3}\right) \times 10^{-2}. \quad (2)$$

After correcting for branching fractions, we obtain

$$\tan^2 \varphi_m \equiv r_\sigma^f = \left(1.1_{-0.7}^{+1.2+6.0}\right) \times 10^{-2} < 0.098 \text{ at } 90\% \text{ C.L.} \quad (3)$$

which translates into a limit of $|\varphi_m| < 17^\circ$ at 90% C.L.

The ratio r_σ^f was predicted to be 1/2 for pure tetraquark states. The measured upper limit on r_σ^f of 0.098 at 90% C.L. deviates from the tetraquark prediction by 8 standard deviations.

1.2. Measurement of resonant components in $\bar{B}_s^0 \rightarrow J/\psi\pi^+\pi^-$ decays

In this analysis, we measure the resonant substructure of the $\bar{B}_s^0 \rightarrow J/\psi\pi^+\pi^-$ decay [4]. The \bar{B}_s^0 signal is shown in Fig. 1 (left). The mass fit gives 27396 ± 207 signal and 7075 ± 101 background candidates, leading to the signal fraction $f_{\text{sig}} = (79.5 \pm 0.2)\%$, within ± 20 MeV of the \bar{B}_s^0 mass peak. A Dalitz plot analysis similar to that used for the \bar{B}^0 has been performed. We find that the data can be described by two solutions, differing on the presence of a non-resonant contribution. The two solutions are displayed in Table II and the fit projection for Solution I is shown in Fig. 2. $f_2(1270)$ and $f_2'(1525)$ contribute with fractions of the order of a few per cent. In both solutions, the $f_0(500)$ state does not have a significant fit fraction. We set an upper limit for the fit fraction ratio between $f_0(500)$ and $f_0(980)$ of 0.3% from Solution I and 3.4% from Solution II, both at 90% C.L. Including uncertainty of $\mathcal{B}(f_0(980) \rightarrow \pi^+\pi^-)$, our limit on the mixing angle is

$$\tan^2 \varphi_m = \frac{\mathcal{B}(\bar{B}^0 \rightarrow J/\psi f_0(500)) \Phi(980)}{\mathcal{B}(\bar{B}^0 \rightarrow J/\psi f_0(980)) \Phi(500)} < 1.8\% \text{ at } 90\% \text{ C.L.} \quad (4)$$

which translates into a limit $|\varphi_m| < 7.7^\circ$ at 90% C.L. The value of $\tan^2 \varphi_m$ is consistent with the tetraquark model, which predicts zero within a few degrees [1].

TABLE II

$\bar{B}_s^0 \rightarrow J/\psi \pi^+ \pi^-$. Fit fractions [%] of the main contributing components for the two Dalitz plot analysis solutions.

Component	Solution I	Solution II
$f_0(980)$	$70.3 \pm 1.5^{+0.4}_{-5.1}$	$92.4 \pm 2.0^{+0.8}_{-16.0}$
$f_0(1500)$	$10.1 \pm 0.8^{+1.1}_{-0.3}$	$9.1 \pm 0.9 \pm 0.3$
$f_0(1790)$	$2.4 \pm 0.4^{+5.0}_{-0.2}$	$0.9 \pm 0.3^{+2.5}_{-0.1}$
NR	—	$5.9 \pm 1.4^{+0.7}_{-4.6}$
Sum	85.2	110.6
$\chi^2/\text{n.d.f.}$	2005/1822	2008/1820

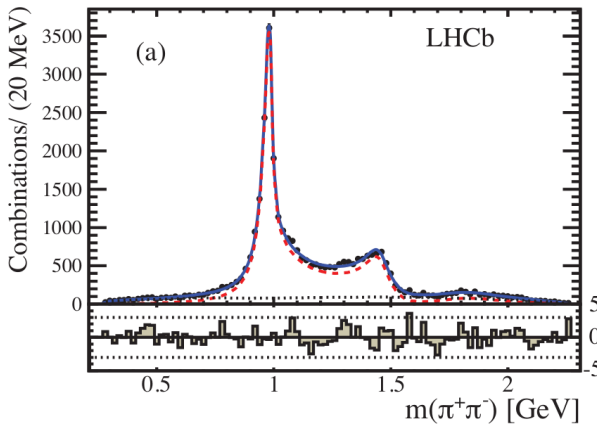


Fig. 2. $\bar{B}_s^0 \rightarrow J/\psi \pi^+ \pi^-$. Fit projection on the $m(\pi^+ \pi^-)$ invariant mass.

1.3. Observation of $\bar{B}_{(s)}^0 \rightarrow J/\psi f_1(1285)$ decays and measurement of the $f_1(1285)$ mixing angle

The $J/\psi \pi^+ \pi^- \pi^+ \pi^-$ invariant mass distribution is shown in Fig. 3 [5]. We fit the mass distribution using the same signal function shape for both \bar{B}_s^0 and \bar{B}^0 peaks. There are 1193 ± 46 \bar{B}_s^0 and 839 ± 39 \bar{B}^0 decays.

The four-pion invariant mass distributions for \bar{B}_s^0 and \bar{B}^0 decays are shown in Fig. 3 (right) where we observe clear $f_1(1285)$ signals.

We obtain the branching fraction ratios, using an efficiency of $0.1820 \pm 0.0036\%$, determined by simulation, for the $J/\psi f_1(1285)$ final state as

$$\frac{\mathcal{B}(\bar{B}^0 \rightarrow J/\psi f_1(1285))}{\mathcal{B}(\bar{B}_s^0 \rightarrow J/\psi f_1(1285))} = \left(11.6 \pm 3.1^{+0.7}_{-0.8}\right)\%. \quad (5)$$

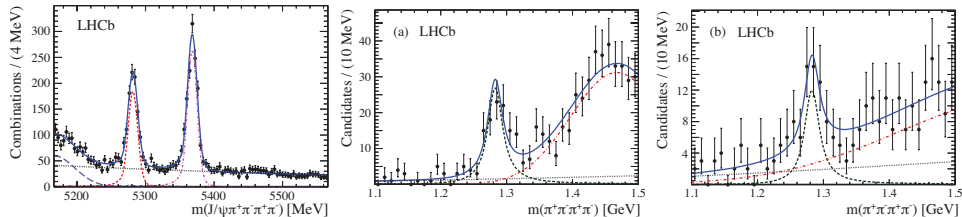


Fig. 3. Left: Invariant mass distribution for $J/\psi \pi^+ \pi^- \pi^+ \pi^-$ combinations. Right: Fits to the four-pion invariant mass in (a) \bar{B}_s^0 and (b) \bar{B}^0 decays.

Our measurement of this ratio differs by 3.3 standard deviations from the tetraquark interpretation including the systematic uncertainty. The resulting mixing angle is

$$\phi = \pm \left(24.0_{-2.6}^{+3.1+0.6} \right)^\circ. \quad (6)$$

2. New results on charm spectroscopy

Charm meson spectroscopy provides a powerful test of the quark model predictions of the Standard Model. Many charm meson states, predicted in the 1980s [6], have not yet been observed experimentally. The J^P states having $P = (-1)^J$ and therefore $J^P = 0^+, 1^-, 2^+, \dots$ are called natural parity states and are labelled as D^* , while unnatural parity indicates the series $J^P = 0^-, 1^+, 2^-, \dots$

2.1. Study of the inclusive production of the $D^+ \pi^-$, $D^0 \pi^+$ and $D^{*+} \pi^-$ systems

This study [7] reports a search for D_J mesons in a data sample, corresponding to an integrated luminosity of 1.0 fb^{-1} . The search for D_J mesons is performed using the inclusive reactions

$$pp \rightarrow D^+ \pi^- X, \quad pp \rightarrow D^0 \pi^+ X, \quad pp \rightarrow D^{*+} \pi^- X, \quad (7)$$

where X represents a system composed of any collection of charged and neutral particles¹.

The charmed mesons in the final state are reconstructed in the decay modes $D^+ \rightarrow K^- \pi^+ \pi^+$, $D^0 \rightarrow K^- \pi^+$ and $D^{*+} \rightarrow D^0 \pi^+$. In order to reduce combinatorial background, the cosine of the angle between the momentum direction of the charged pion in the $D^{(*)} \pi^\pm$ rest frame and the momentum direction of the $D^{(*)} \pi^\pm$ system in the laboratory frame is required to be greater than zero. We require $p_T(D^{(*)} \pi) > 7.5 \text{ GeV}$ and obtain 7.9×10^6 , 7.5×10^6 and 2.1×10^6 $D^+ \pi^-$, $D^0 \pi^+$ and $D^{*+} \pi^-$ candidates.

¹ Use of charge-conjugate decay modes is implied.

The $D^+\pi^-$ mass spectrum, Fig. 4 (left), shows a double peak structure around 2300 MeV due to cross-feed from the decay $D_1(2420)^0$ or $D_2^*(2460)^0 \rightarrow \pi^- D^{*+} (\rightarrow D^+\pi^0/\gamma)$, where the π^0/γ is not reconstructed. We observe a strong $D_2^*(2460)^0$ signal and weak structures around 2600 and 2750 MeV. The $D^0\pi^+$ mass spectrum, Fig. 4 (right), shows an enhanced double peak structure around 2300 MeV due to cross-feed from the decays $D_1(2420)^+$ or $D_2^*(2460)^+ \rightarrow \pi^+ D^{*0} (\rightarrow D^0\pi^0/\gamma)$. The $D_2^*(2460)^+$ signal and weak structures around 2600 and 2750 MeV are observed. The $D^{*+}\pi^-$ mass spectrum, shown in Fig. 5, is dominated by the presence of the $D_1(2420)^0$ and $D_2^*(2460)^0$ signals. At higher mass, complex broad structures are evident in the mass region between 2500 and 2800 MeV.

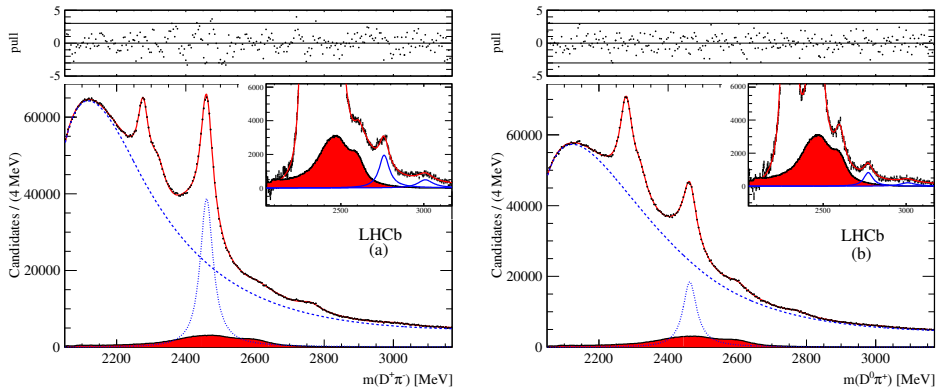


Fig. 4. Fit to the $D^+\pi^-$ mass spectrum (left) and to the $D^0\pi^+$ mass spectrum (right). The filled histogram (dark grey/red) shows the estimated cross-feeds from the high mass $D^*\pi$ resonances.

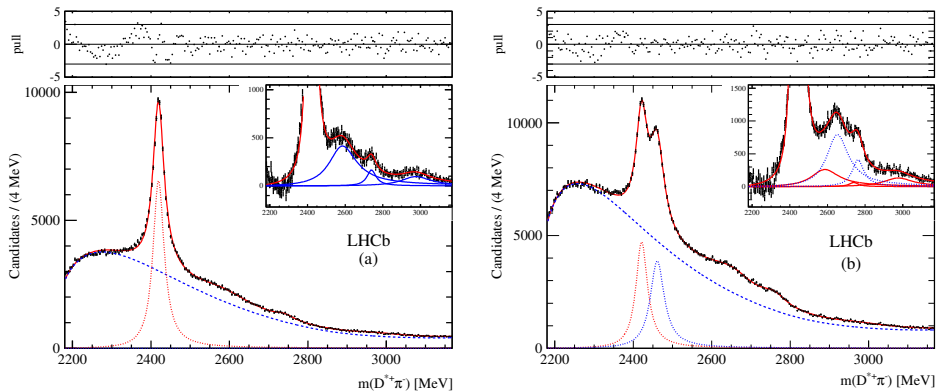


Fig. 5. Fit to the $D^{*+}\pi^-$ mass spectrum, *enhanced unnatural parity sample* (left) and *natural parity sample* (right).

We define the helicity angle θ_H as the angle between the π^- and the π^+ from the D^{*+} decay, in the rest frame of the $D^{*+}\pi^-$ system. We define *enhanced unnatural parity sample* the sample selected by the condition $|\cos\theta_H| > 0.75$ and *natural parity sample* the sample selected by the condition $|\cos\theta_H| < 0.5$. It is expected that the angular distributions are proportional to $\sin^2\theta_H$ for natural parity resonances and proportional to $1 + h\cos^2\theta_H$ for unnatural parity resonances, where $h > 0$ is a free parameter. The $D^*\pi$ decay of a $J^P = 0^+$ resonance is forbidden.

The data and fit for the $D^{*+}\pi^-$ *enhanced unnatural parity sample* are shown in Fig. 5 (left) and the resulting fit parameters are summarized in Table III. To obtain a good fit to the mass spectrum, three further unnatural parity resonances, $D_J(2580)^0$, $D_J(2740)^0$, and $D_J(3000)^0$ are needed. We fix masses and widths of the unnatural parity resonances and fit the *natural parity sample* in Fig. 5 (right). To obtain a good fit, two additional resonances, $D_J^*(2650)^0$ and $D_J^*(2760)^0$ are needed. All the statistical significances are well above 5σ .

TABLE III

Resonance parameters, yields and statistical significances.

Resonance	Final state	Mass [MeV]			Width [MeV]			Significance
$D_J^*(2650)^0$	$D^{*+}\pi^-$	2649.2 ± 3.5	± 3.5		140.2 ± 17.1	± 18.6		24.5
$D_J^*(2760)^0$	$D^{*+}\pi^-$	2761.1 ± 5.1	± 6.5		74.4 ± 3.4	± 37.0		10.2
$D_J(2580)^0$	$D^{*+}\pi^-$	2579.5 ± 3.4	± 5.5		177.5 ± 17.8	± 46.0		18.8
$D_J(2740)^0$	$D^{*+}\pi^-$	2737.0 ± 3.5	± 11.2		73.2 ± 13.4	± 25.0		7.2
$D_J(3000)^0$	$D^{*+}\pi^-$	2971.8 ± 8.7			188.1 ± 44.8	9.0		
$D_J^*(2760)^0$	$D^+\pi^-$	2760.1 ± 1.1	± 3.7		74.4 ± 3.4	± 19.1		17.3
$D_J^*(3000)^0$	$D^+\pi^-$	3008.1 ± 4.0			110.5 ± 11.5			21.2
$D_J^*(2760)^+$	$D^0\pi^+$	2771.7 ± 1.7	± 3.8		66.7 ± 6.6	± 10.5		18.8
$D_J^*(3000)^+$	$D^0\pi^+$	3008.1	(fixed)		110.5	(fixed)		6.6

To obtain information on the spin-parity assignment of the states observed in the $D^{*+}\pi^-$ mass spectrum, we subdivide the data into ten equally spaced bins in $\cos\theta_H$ which are fitted with fixed resonance parameters. The resulting yields for $D_1(2420)^0$ and $D_2^*(2460)^0$ are shown in Fig. 6 (a)–(b). A good description of the data is obtained in terms of the expected angular distributions for $J^P = 1^+$ and $J^P = 2^+$ resonances. Figure 6 (c)–(d) shows the resulting distributions for the $D_J^*(2650)^0$ and $D_J^*(2760)^0$ states. In both cases, the distributions are best fitted by the natural parity hypothesis. Figure 7 shows the angular distributions for the $D_J(2580)^0$, $D_J(2740)^0$ and $D_J(3000)^0$ states. The distributions are fitted with natural parity and unnatural parity. In all cases, unnatural parity is preferred over a natural parity assignment. The fits to the $D^+\pi^-$ and $D^0\pi^+$ mass spectra, where only natural parity resonances are allowed, are shown in Fig. 4 (left) and

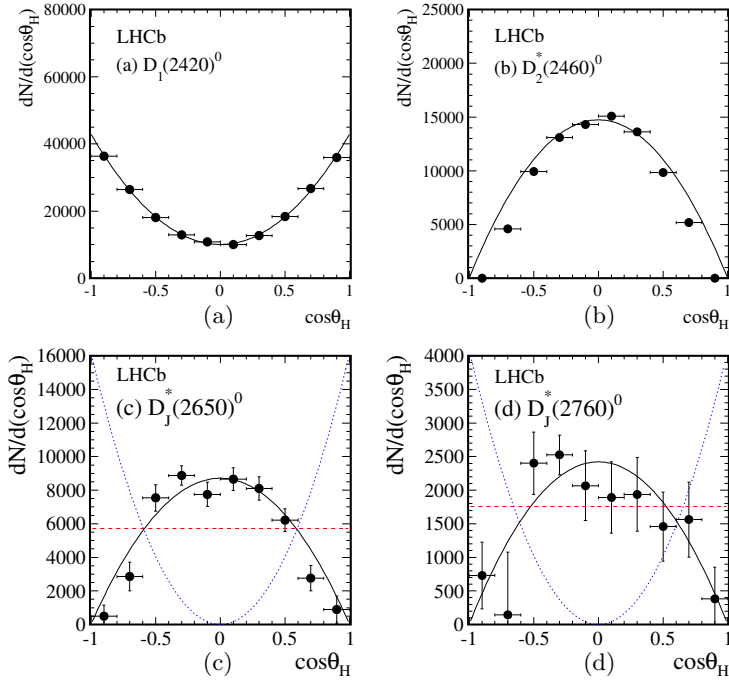


Fig. 6. Distributions of (a) $D_1(2420)^0$, (b) $D_2^*(2460)^0$, (c) $D_J^*(2650)^0$ and (d) $D_J^*(2760)^0$ candidates as functions of the helicity angle $\cos\theta_H$. The distributions are fitted with natural parity (solid/black), unnatural parity (dashed/red) and $J^P = 0^-$ (dotted/blue) functions.

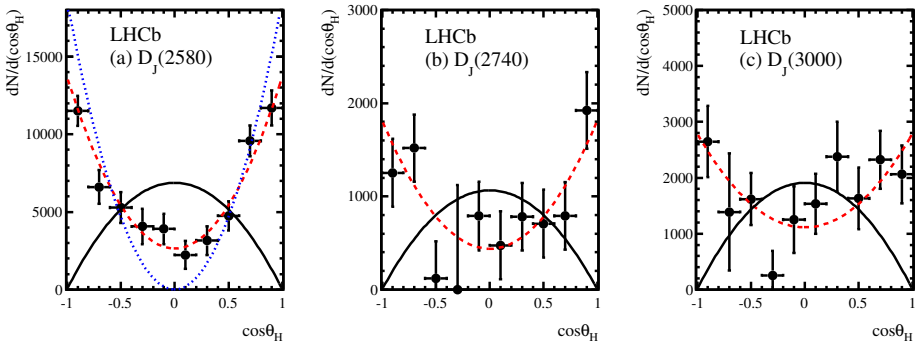


Fig. 7. Distributions of (a) $D_J(2580)^0$, (b) $D_J(2740)^0$ and (c) $D_J(3000)^0$ candidates as functions of the helicity angle $\cos\theta_H$. The distributions are fitted with natural parity (solid/black), unnatural parity (dashed/red) and $J^P = 0^-$ (dotted/blue) functions.

(right). The figures also show the cross-feeds originating from the complex resonance structure present in the $D^*\pi$ mass spectrum in the mass region between 2500 and 2800 MeV. This makes difficult the determination of the $D_J^*(2650)^0$ parameters. To obtain good quality fits, we add broad structures around 3000 MeV, which we label $D_J^*(3000)^0$ and $D_J^*(3000)^+$.

2.2. Observation of overlapping spin-1 and spin-3 $\bar{D}^0 K^-$ resonances at mass 2.86 GeV/c

A Dalitz plot analysis of $B_s^0 \rightarrow \bar{D}^0 K^- \pi^+$ has been performed [8]. The B_s^0 signal has been isolated using BDT algorithms and is shown in Fig. 8 (left). The signal region contains 12 954 of which $11\,302 \pm 159$ are signal decays. The Dalitz plot distribution of the candidates in the signal region, shown in Fig. 8 (right), is fitted with a model that includes both signal and background components. The largest components in terms of their fit fractions, defined as the ratio of the integrals over the Dalitz plot of a single decay amplitude squared and the total amplitude squared, are the $\bar{K}^*(892)^0$ (28.6%), $D_{s2}^*(2573)^-$ (25.7%), LASS (21.4%) and $\bar{D}^0 K^-$ non-resonant (12.4%) terms. The fit fractions for the $D_{s1}^*(2860)^-$ and $D_{s3}^*(2860)^-$ components are $(5.0 \pm 1.2 \pm 0.7 \pm 3.3)\%$ and $(2.2 \pm 0.1 \pm 0.3 \pm 0.4)\%$, respectively, where the uncertainties are statistical, systematic and from Dalitz plot model variations. To assess the significance of the two states near $m(\bar{D}^0 K^-) \approx 2860$ MeV/c², the fit is repeated with either one or two resonant amplitudes with different spins. The statistical significances of the spin-3 and spin-1 components are found to be 16.4 and 15.3 standard deviations, respectively. Figure 9 shows the data and fit projections onto the $\bar{D}^0 K^-$ mass with a zoom in Fig. 9 (e) of the $D_{s,J}^*(2860)^-$ region. The masses and widths of the $D_{s2}^*(2573)^-$, $D_{s1}^*(2860)^-$ and $D_{s3}^*(2860)^-$ states are given in Table IV. The results support an interpretation of these states being the $J^P = 1^-$ and 3^- members of the 1D family.

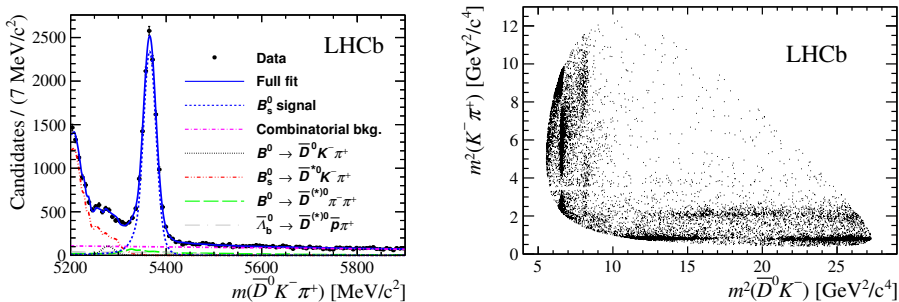


Fig. 8. Left: Fit to the $B_s^0 \rightarrow \bar{D}^0 K^- \pi^+$ candidate invariant mass distribution. Right: Dalitz plot distribution in the B_s^0 signal region.

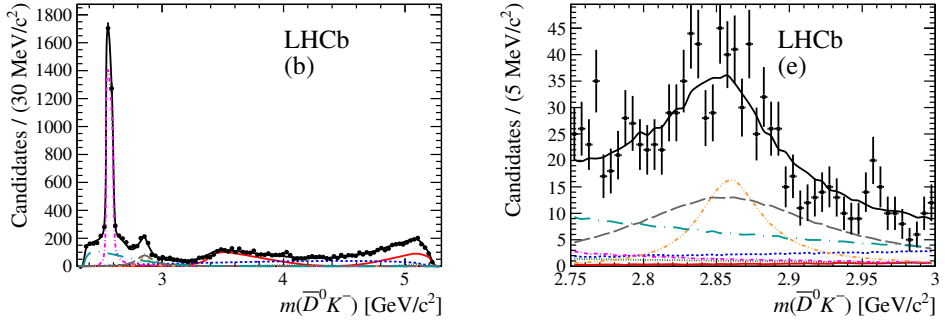


Fig. 9. Projections of the data and the Dalitz plot fit result onto (b) $m(\bar{D}^0 K^-)$ with a zoom into (e) the $D_{sJ}^*(2860)^-$ region.

TABLE IV

Resonances parameters from the Dalitz analysis of $B_s^0 \rightarrow \bar{D}^0 K^- \pi^+$.

Resonance	Mass [MeV]	Width [MeV]
$D_{s2}^*(2573)^-$	$2568.39 \pm 0.29 \pm 0.19 \pm 0.18$	$16.9 \pm 0.5 \pm 0.4 \pm 0.4$
$D_{s1}^*(2860)^-$	$2859 \pm 12 \pm 6 \pm 23$	$159 \pm 23 \pm 27 \pm 72$
$D_{s3}^*(2860)^-$	$2860.5 \pm 2.6 \pm 2.5 \pm 6.0$	$53 \pm 7 \pm 4 \pm 6$

REFERENCES

- [1] S. Stone, L. Zhang, *Phys. Rev. Lett.* **111**, 062001 (2013).
- [2] R. Aaij *et al.* [LHCb Collaboration], *Phys. Rev.* **D90**, 012003 (2014).
- [3] A. Hocker *et al.*, *PoS ACAT*, 040 (2007).
- [4] R. Aaij *et al.* [LHCb Collaboration], *Phys. Rev.* **D89**, 092006 (2014).
- [5] R. Aaij *et al.* [LHCb Collaboration], *Phys. Rev. Lett.* **112**, 091802 (2014).
- [6] S. Godfrey, N. Isgur, *Phys. Rev.* **D32**, 189 (1985).
- [7] R. Aaij *et al.* [LHCb Collaboration], *J. High Energy Phys.* **09**, 145 (2013).
- [8] R. Aaij *et al.* [LHCb Collaboration], *Phys. Rev. Lett.* **113**, 162001 (2014).